Catalysis Today 180 (2012) 9–18

Contents lists available at ScienceDirect

Catalysis Today

journal homepage: www.elsevier.com/locate/cattod

Infrared spectroscopic study of carbon dioxide adsorption on the surface of cerium–gallium mixed oxides

Gisela Finos[a], Sebastián Collins[a,*], Ginesa Blanco[b], Eloy del Rio[b], José María Cíes[b], Serafín Bernal[b], Adrian Bonivardi[a]

[a] Instituto de Desarrollo Tecnológico para la Industria Química (INTEC) CONICET-UNL, Güemes 3450, 3000 Santa Fe, Argentina
[b] Dpto. de Ciencias de los Materiales, Ingeniería Metalúrgica y Química Inorgánica, Facultad de Ciencias, Universidad de Cádiz, Puerto Real E11510, Spain

ARTICLE INFO

Article history:
Available online 11 June 2011

Keywords:
Cerium oxide
Gallium oxide
Carbonate species
Infrared spectroscopy

ABSTRACT

In order to modified the acid–base properties of pure cerium dioxide, a series of ceria-based oxides doped with gallium(III) cations (from 5 to 50% mol/mol of Ga) was prepared by co-precipitation in basic aqueous solution followed by calcination at 773 K. N_2 physisorption at 77 K showed that mesoporous materials with surface areas between 75 and 104 m^2/g were obtained. Ga(III) cations were incorporated into the ceria crystal structure up to a concentration close to 20–25% mol/mol of Ga, as revealed by powder X-ray diffraction analysis. Surface basicity was investigated using CO_2 chemisorption by mass spectrometry and in situ infrared spectroscopy. A progressive decrease in the surface basicity in the series of ceria–gallia materials was observed as the Ga content increases. Different carbonate and bicarbonate surface species were identified through their vibrational infrared modes. A remarkable decrease in the surface stability of carbonate species, particularly of the polydentate carbonate groups, was detected, which is correlated to the incorporation of gallium(III) into the ceria lattice.

1. Introduction

It is well known that CeO_2 is widely used as a component or active phase in numerous redox catalytic processes [1]. Among many other important reactions, CeO_2-supported noble metal (Au, Pt) materials are promising catalysts for two key processes in high purity hydrogen production for fuel cell applications, that is, the low-temperature water gas shift (LTWGS) reaction, and the preferential oxidation of CO in a H_2 rich stream (PROX) [2–4]. However, a major problem currently found in the ceria-based catalysts for the pure hydrogen production mentioned above is their progressive deactivation under reaction conditions [5–7]. Among several others [5,8], poisoning effects due to carbonate species strongly adsorbed on the ceria surface, have been considered a major cause of deactivation [5,9,10].

Therefore, some of us have already claimed that the development of unconventional ceria-based oxide supports forming more labile carbonate species, while keeping the appropriate redox behavior, represents an attractive target for research [11]. This lead us to initiate a research project to evaluate the textural, structural, acid–base, and redox properties of materials resulting from the addition of gallia to cerium dioxide, that is, using a more acidic oxide to tune the surface acid–base properties of the support.

Doping ceria with alio-cations is known to be an efficient and versatile way of modulating the textural, structural and chemical properties of the pure oxide [1]. In most of cases, however, the doping cations consisted of lanthanoids and closely related elements like yttrium [12]. However, the incorporation of M^{3+} cations in ceria-based mixed oxides, such as B, Al, Ga and In, have been reported recently [13,14]. Moreover, some of us have proved that it is possible to incorporate Ga(III) cations (25% mol/mol) into the lattice of cubic cerium oxide. That incorporation of gallium(III) into the ceria lattice produced strong modifications of the redox and acid-basic properties of Ce–Ga system [11]. Temperature-programmed reduction experiments, with H_2 or CO, showed that the redox behavior of ceria was noticeably enhanced after doping the pure ceria with 25% mol/mol of gallium. Additionally, that cerium–gallium mixed oxide presented a lower uptake of CO_2 and CO, which was correlated with a loss of stronger surface basic sites after the Ga(III) addition to CeO_2.

Acidity and basicity are concepts frequently used to explain the catalytic properties of different materials [15]. The number, nature, strength and location of the acid–base active sites are important parameters to achieve correlations between catalytic activity and surface properties in catalysis. To this end, a large number of physicochemical methods have been developed. The adsorption of basic probe molecules, such as pyridine or related molecules, is used to evaluate acid sites. Conversely, carbon dioxide is frequently used to investigate surface basic centers [15–19]. CO_2 chemisorbs on O^{2-} and HO^- surface basic sites producing carbonate and bicarbonate

* Corresponding author.
E-mail address: scollins@santafe-conicet.gov.ar (S. Collins).

0920-5861/$ – see front matter © 2011 Elsevier B.V. All rights reserved.
doi:10.1016/j.cattod.2011.04.054

species. These last (bi)carbonate groups are also of great interest as intermediate (or spectators) species in the CO oxidation or WGS reactions [5,8,20]. Moreover, some of those carbonate have been considered as poison. For instance, strongly bond hydroxycarbonate species have been proposed as responsible of the ceria-based catalysts deactivation during WGS reaction [5,8].

The identification of each (or most) of the carbonate groups formed on a catalyst surface can be accomplished by using infrared (IR) spectroscopy [15,20]. In particular, several authors have worked on the identification of carbonaceous species generated on cerium oxide after CO and CO_2 adsorption employing Fourier transform IR spectroscopy. Among them, the works of Lavalley and coworkers [15–17] and Li et al. [18,19] deserve a special attention due to the detailed assignment of IR bands to different surface carbonate species on ceria.

Thus, it seems reasonable to study how the progressive incorporation of gallium(III) can modify acid–base properties of ceria. In this work, a series of Ce–Ga oxides with a broad range of gallium concentration was investigated, mainly by IR spectroscopy, in order to identify and characterize the surface carbonate species formed upon carbon dioxide adsorption. The thermal stability of those carbonate groups was also evaluated by means of temperature-programmed desorption experiments.

2. Experimental

2.1. Sample preparation

Cerium–gallium oxides with increasing molar amount of gallium (nominal compositions $Ce_{1-x}Ga_xO_{2-x/2}$, with x: 0.05, 0.10, 0.20, 0.25 and 0.50) have been prepared and characterized (Table 1). Additionally, pure cerium(IV) and gallium(III) oxides were used as reference materials.

Ce–Ga oxides were prepared by precipitation with aqueous ammonium hydroxide from the appropriate solutions in purified water (18 ΩM) of the corresponding nitrates, $Ce(NO_3)_3{\cdot}6H_2O$ (99.99%, Aldrich) and $Ga(NO_3)_3{\cdot}9H_2O$ (99.999%, Aldrich) at room temperature. A solution containing both metal cations was dropwise added to an ammonia solution pH 10. Then, the pH of the suspension was controlled in the range of 8.0–8.5 by co-adding aqueous ammonia solution (14 wt%). The complete precipitation of gallium(III) and cerium(III) cations was verified in a previous work of some of us [11]. The resulting solids were centrifuged at 5000 rpm for 20 min, washed with purified water (six-times the solid volume), dried in air at 343 K for 8 h, and finally calcined at 773 K for 5 h.

Pure CeO_2 was obtained by following the same procedure described above. Pure γ-Ga_2O_3 phase was prepared following the procedure reported elsewhere [21]. Hydrated gallium hydroxide gel was obtained from the addition of an ammonia ethanolic solution (14 wt%) to a solution of $Ga(NO_3)_3{\cdot}9H_2O$ in ethanol. This gel was filtered and washed with ethanol at room temperature. The gallium oxide was obtained after drying (343 K, 8 h), and calcining (773 K, 5 h) the previous precipitate.

2.2. Characterization

The structural nature of the phases presented in the calcined samples was determined by X-ray diffraction spectrometry (XRD). A Shimadzu XD-D1 apparatus (Cu Kα radiation, 0.125°/min) was used for this study.

A Micromeritics ASAP 2020 instrument was used to measure the Brunauer–Emmett–Teller (BET) surface area (S_{BET}) of the oxides. Prior to measure the N_2 adsorption isotherms at 77 K, the sam-

Table 1
Composition, structure and morphology of the cerium–gallium oxide samples.

Code	Gallium content, Ga/(Ce + Ga) (% mol/mol)		S_{BET}[c] (m^2/g)	S_M[d] (cm^2/mol)	Mean pore diameter[e] (nm)	Pore volume (cm^3/g)	Crystal phase	Mean crystal size[f] (nm)	Lattice parameter (nm)
	Nominal[a]	Surface[b]							
CeO_2	0	–	83	1.43	7.6	0.153	Cubic fluorite (Fm3m)	10.8	0.5411
CeGa05	5	4.3	94	1.58	5.5	0.165	Cubic fluorite (Fm3m)	6.7	0.5392
CeGa10	10	8.1	97	1.59	5.1	0.158	Cubic fluorite (Fm3m)	4.7	0.5386
CeGa20	20	15.6	104	1.63	5.5	0.178	Cubic fluorite (Fm3m)	3.3	0.5383
CeGa25	25	18.1	102	1.56	4.5	0.148	Cubic fluorite (Fm3m)	3.2	0.5384
CeGa50	50	27.8	75	1.00	3.7	0.085	Cubic fluorite (Fm3m)	2.9	0.5385
Ga_2O_3	100	–	126	2.46	3.5	0.117	Gamma, spinel-type (Fd3m)	1.8	–

[a] Bulk composition.
[b] Determined from the Ga 2p and Ce 3d XPS signals.
[c] Surface area measured by the Brunauer–Emmett–Teller method at 77 K.
[d] Surface area per mol of oxide assuming the nominal composition.
[e] Calculated by the Barrett–Joyner–Halenda (BJH) method from the desorption isotherm.
[f] As determined from line broadening of the (1 1 1) diffraction peaks of CeO_2 by using the Debye–Scherrer equation.

ples were outgassed at 473 K for 2 h under dynamic vacuum (base pressure = 1×10^{-6} Torr).

X-ray photoelectron spectroscopy (XPS) studies were carried out in a XPS spectrometer, Kratos Axis Ultra DLD. A self-supported wafer of each pure oxide and Ce–Ga mixed oxides were successively place into the vacuum chamber of the spectrometer. Spectra were recorded with monochromatic AlKα radiation (1486.6 eV) with a selected X-ray power of 150 W. The spectrometer was operated in the fixed analyzer transmission (FAT) mode with a pass energy equal to 20 eV. Surface charging effects were compensated by using the Kratos coaxial neutralization system. The binding energy (BE) scale was calibrated with respect to the C 1s signal and fixed to 285.0 eV. Spectral processing was performed with CasaXPS software. Integration of the Ce and Ga signals was carried out by using a Tougaard and Shirley-type background lines, respectively.

CO_2 adsorption, at 298 K, was investigated by in situ transmission Fourier transform infrared (IR) spectroscopy on self-supported disks (30 mg) of the oxide samples pressed at 5 t cm^{-2} (wafer diameter = 13 mm). The sample wafers were placed into a Pyrex IR cell fitted with water-cooled NaCl windows, which was attached to a conventional high vacuum system (base pressure = 1×10^{-4} Torr), equipped with a manifold for gas flow operation. Before the adsorption of CO_2, the samples were cleaned as follows: (1) heating from 298 K to 723 K (10 K min^{-1}) in a flow of pure H_2 (50 cm^3 min^{-1}), (2) evacuation at 723 K during 15 min; (3) re-oxidation under flowing O_2 (50 cm^3 min^{-1}) at 723 K for 15 min, (4) cooling to 398 K still under oxygen flow, (5) evacuation at 398 K during 25 min, and (6) cooling to 298 K under dynamic vacuum. This cleaning procedure was considered to be the best option to thoroughly remove the surface carbonates from these oxide materials. Carbon dioxide adsorption isotherms were recorded at 298 K by progressively increasing the CO_2 partial pressure up to 760 Torr. The cell was then evacuated for 30 min and, subsequently, a temperature-programmed desorption (TPD) experiment was run by heating the IR cell from 298 to 723 K (10 K min^{-1}). No change in the surface area and/or the original XRD pattern of any of the samples was detected after the in situ TPD experiments.

The in situ transmission IR spectra were registered employing a Magna 550 FTIR spectrometer with a MCT cooled detector (4 cm^{-1} resolution, 100 scans). Background correction of the spectra was achieved by subtracting the spectra of the pretreated wafers at each temperature; a Lorentzian sum function was used to fit the overlapping bands and to measure peak areas and/or intensities.

Quantitative CO_2 uptake at 298 K was also determined by using a micro-reactor coupled on-line with a Baltzers QMG 421 quadrupole mass spectrometer. Approximately 200 mg of the oxide samples diluted with 200 mg of crushed quartz, 80–30 mesh, were first submitted to a cleaning procedure similar to that reported above, in which steps 5 and 6 consisted of treatments under flowing He, instead of high vacuum. The amount of adsorbed CO_2 on the oxides was determined at 298 K after switching a chromatographic valve from pure He to 5%CO_2/Ar (10 cm^3 min^{-1}). The total CO_2 uptake (Q), under a partial pressure of 37 Torr of the adsorbate (equilibrium condition), was determined by taking the integral of the difference between the trace of the adsorbate during the adsorption experiment (curve_ads) and the trace of a blank experiment (curve_blank), for a given gas molar flow rate of the adsorbate (F) and weight of sample (W) from $t = 0$ s to $t = 300$ s.

$$Q = \int_{o}^{ta} (\text{curve\_ads} - \text{curve\_blank}) \cdot \frac{F}{W}\, dt$$

All the gases used in this work were high purity grade and were further purified as follows: H_2 (Indura, 5.0), He (Indura, 5.0), and CO_2 (Indura, 4.6) were passed through MnO/Al_2O_3 and molecular sieve (3 Å, Fisher Co.) traps to eliminate oxygen and water impurities, respectively; O_2 (AGA, 5.0) was passed through a molecular sieve (3 Å, Fisher Co.) and Ascarite traps to remove water and carbon dioxide, respectively.

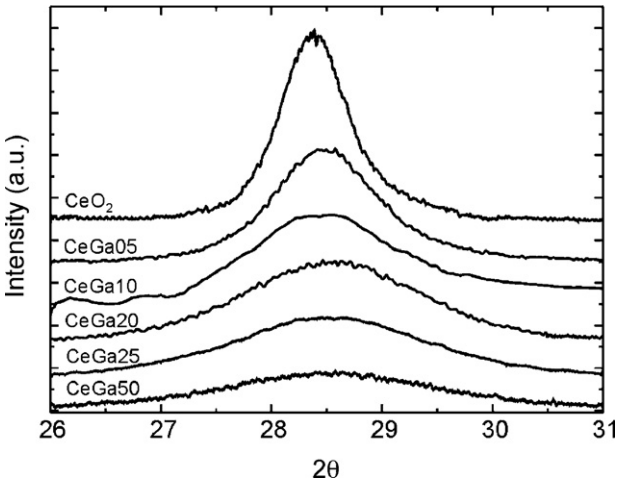

Fig. 1. X-ray diffraction pattern of the Ce–Ga oxides.

3. Results and discussion

3.1. Structural and chemical characterization

Table 1 summarizes the nominal chemical composition and textural properties of the cerium–gallium oxide samples including pure ceria and gallia as reference materials. All the materials are mesoporous (mean pore diameter = 3.5–7.6 nm) with moderate BET surface areas (75–126 m^2/g). The addition of gallium to ceria produces a slightly increase of the surface area per weight of the oxide as long as the amount of gallium content increases, except for the CeGa50 sample. However, based on the molecular weight of the oxides, the values of BET surface areas can be corrected to express the surface area per mol of oxide. These new molecular surface areas are very similar up to 25% mol/mol of Ga. Only a 30% decreased of the molecular surface area is observed for the CeGa50 material together with a reduction of the pore volume. These findings are in agreement with the formation of cerium–gallium mixed oxides for gallium concentration lower than 25% mol/mol [11], and with phase segregation for higher gallia loadings, as it is shown below.

The crystal structure of the set of solids was studied by powder XRD. Pure ceria shows the characteristic peaks of a cubic, fluorite-type, structure (JCPDS 34-0394), while pure gallia depicts the typical broad diffraction peaks assigned to the γ-polymorph with cubic, spinel-type, structure [21,22]. In the case of the Ce–Ga oxide samples, the only diffraction peaks that could be observed were those due to the fluorite structure.

The comparison among the (1 1 1) diffraction peak positions in the XRD patterns for the cerium based oxides is presented in Fig. 1. As deduced from their full width at half maxima, peaks in ceria–gallia patterns are significantly broader than those for pure ceria, indicating a decrease in the mean crystal size in the mixed oxide samples (Table 1). Also, a consistent shift toward higher 2θ angles is observed for that diffraction line, as compared to the one of CeO_2, of the gallium-doped samples with gallium content lower than 25% mol/mol. This shift is in agreement with a size reduction of the crystal cell due to the incorporation of the Ga^{3+} dopant with a lower ionic radius ($r_{Ga^{3+}} = 0.062$ nm) in exchange of Ce^{4+} ($r_{Ce^{4+}} = 0.097$ nm) and the loss of oxygen anion for charge balance [1]. In other words, the decrease of the lattice parameter observed in Table 1 confirms previous results of some of us

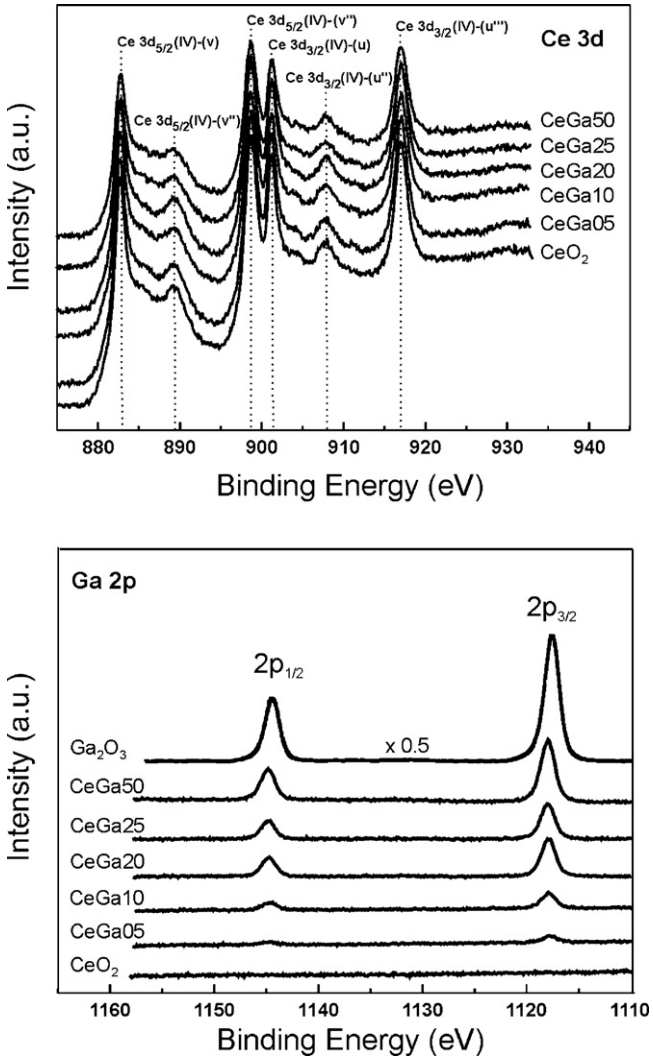

Fig. 2. Ce 3d and Ga 2p XPS spectra of the CeO_2, Ga_2O_3, and Ce–Ga oxides.

where homogenous cerium–gallium mixed oxide were obtained for concentrations equals to 20 and 25% mol/mol of Ga [11,23].

Thus, it is possible to conclude that the substitution of Ce^{4+} cations by Ga^{3+} takes place into the ceria matrix for gallium loading equal or lower than 25% mol/mol, leading to materials with similar molar surface area.

To determine the surface composition of the oxides, the XPS spectra of Ga (2p), Ce (3d), O (1s) and C (1s) were recorded. Fig. 2 shows the XPS spectra for the Ce 3d and Ga 2p signals. It is clear that the intensity of the Ce 3d peaks decreases with the gallium content into the sample, while the opposite is true for the Ga 2p peaks. Table 1 shows the results of the quantitative analysis of the surface Ga/(Ga + Ce) ratio. Although, this technique is surface sensitive, it is well known that the real depth of analysis depends on the photon energy of the incident radiation and the binding energy (BE) of electrons emitted by the sample [24]. In our case, for an incident energy equal to 1486.6 eV and BEs between 880 and 1145 eV, a depth of analysis from 3 to 6 nm, which is equivalent to an average of 8 unit cells, was estimated. Thus, the surface Ga/(Ga + Ce) ratio, as determined by XPS, shows a "surface" enrichment in cerium for Ce–Ga oxide samples as compare to the nominal or bulk composition. Particularly, the CeGa50 sample presents the most deviated surface Ga/(Ga + Ce) ratio value, which can be an indication of oxide phase segregation.

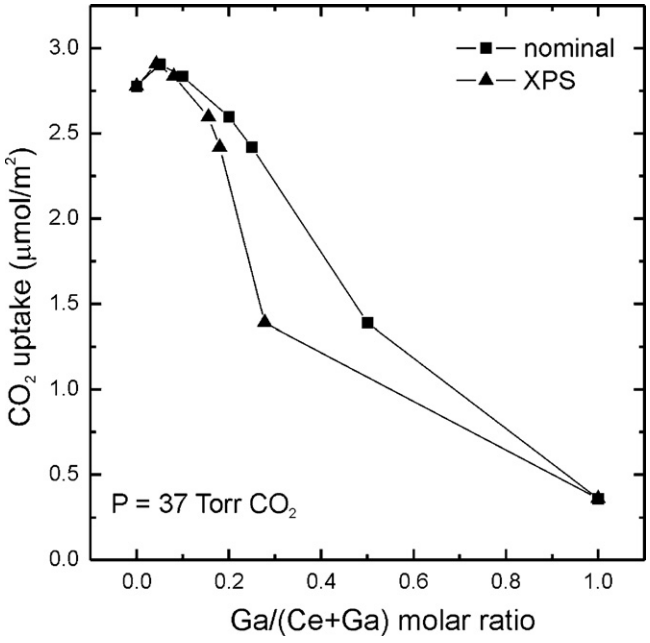

Fig. 3. Total amount of CO_2 adsorbed under dynamic conditions at 298 K, as determined by MS, versus the bulk (nominal) and surface (XPS) Ga/(Ce + Ga) molar ratio.

3.2. Uptake of carbon dioxide by mass spectrometry

Fig. 3 depicts the total amount of CO_2 uptake on the cleaned oxide samples measured at 298 K, under dynamic conditions, at a constant partial pressure of the adsorbate (37 Torr CO_2). The CO_2 uptake decreases, from approximately 2.8 to 0.4 μmol/m^2 (from pure CeO_2 to Ga_2O_3, respectively), as the gallium content into the samples increases. This trend seems similar either considering the nominal or XPS gallium loading. However, it is observed that the CO_2 adsorption is strongly affected for the presence of gallium on the surface of the mixed oxides because of the lack of a linear correlation between the CO_2 uptake and the gallium content. Then, it is proposed that the amount and type of surface basic site for the adsorption of the CO_2 molecule have been modified by the incorporation of Ga^{3+} into the ceria lattice. First, the presence of oxygen vacancies after the incorporation of Ga^{3+} into the ceria lattice was suggested in a previous work [11], and it seems reasonable to expect that these vacancies would alter the capacity of the mixed oxide to adsorb carbon dioxide. Second, the type of basic site, mainly O^{2-} site, might strongly change since more ionic Ce–O–Ce surface bonds are being partially replaced by more covalent Ce–O–Ga surface bonds, as showed by preliminary DFT theoretical results [25]. Moreover, it will be showed below that the type of carbonate species over the surface of the powder mixed oxides is affected by the surface amount of gallium. Therefore, it is not straightforward to find an explanation of the non-linear variation of the CO_2 uptake with gallium loading, which is more remarkable for the CeGa50, that is, a heterogeneous material.

Now, to understand the nature of the CO_2 adsorption infrared spectroscopy was extensively applied not only to identify of the various surface carbonate species but also to compare their thermal stability.

3.3. Surface carbonate species by infrared spectroscopy

The surface carbonate groups were investigated by the adsorption of CO_2 at different pressures and by temperature programmed desorption experiments by using in situ infrared spectroscopy.

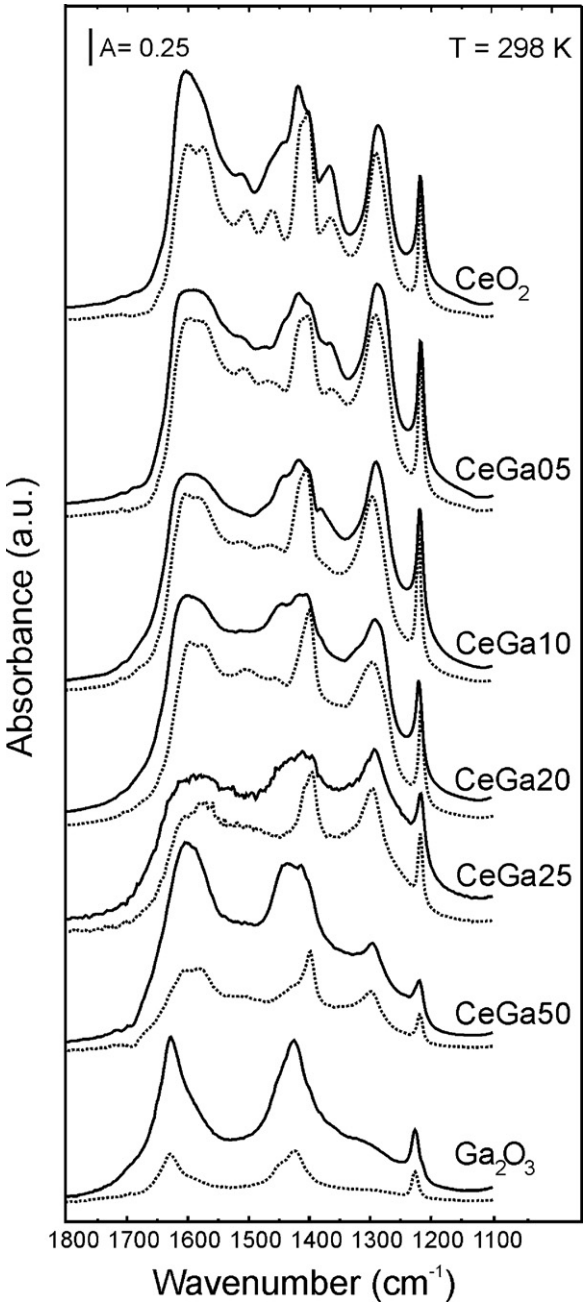

Fig. 4. Infrared spectra after the CO_2 adsorption at 1 (dotted line) and 760 (solid line) Torr on the CeO_2, Ga_2O_3, and Ce–Ga oxides at 298 K. The spectra were corrected by wafer weight and surface area of each sample.

The CO_2 isothermal adsorption over the clean wafer of the oxides was carried out at 298 K. The infrared spectra were recorded at increasing partial pressure of CO_2 from 1 to 760 Torr. Fig. 4 shows the IR spectra taken at lowest and highest CO_2 pressure. The infrared bands show the formation of several and different types of carbonate (including bicarbonate) species whose proportions appear to change gradually with the gallium addition to the ceria matrix. But the relative amount of those species seems to be slightly modified after increasing the pressure of CO_2.

Fig. 5 summarizes the adsorption isotherms built up by plotting the total integrated IR absorbance data for the spectral region ranging from 1800 to 1100 cm^{-1} versus the corresponding CO_2 partial pressure at which the spectra were recorded. Langmuir-type isotherms were obtained on the whole set of samples, where

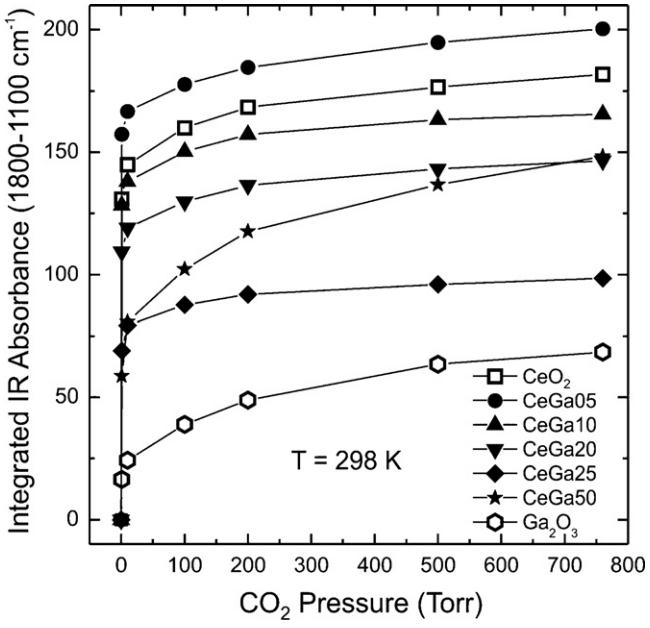

Fig. 5. Isothermal CO_2 adsorption on ceria–gallia samples measured by infrared absorption in the 1800–1100 cm^{-1} region as a function of the equilibrium pressure of CO_2 gas. The spectra were corrected by wafer weight and surface area of each sample.

the saturation coverage was reached over approximately 10 Torr of CO_2. Next, it is possible to assume that the carbonate groups were essentially formed over the surface of the oxides.

Fig. 5 also reveals that the concentration of the surface carbonates species depends on the gallium loading. In general, while the concentration of gallium oxide increases (an amphoteric material), or the concentration of ceria decreases (a basic oxide), the surface concentration of carbonate groups decreases. However, in order to get a better understanding of the CO_2 chemisorption, the normalized integrated infrared absorbance or normalized IR area of the carbonate species was plotted against the normalized amount of absorbed CO_2 measured by mass spectrometry (MS) in Fig. 6. The IR area where calculated by interpolation at 37 Torr CO_2 assuming a linear variation between the experimental points of IR absorbance at 10 and 100 Torr. Only if the surface carbonate species have identical IR absorption coefficients and/or similar relative concentrations do the experimental points in Fig. 6 rest over the straight line of slope equal to 1. Certainly, one or both conditions are not satisfied, within the experimental errors, at least for the homogenous cerium–gallium mixed oxides. For example, the increment of gallium concentration in those mixed oxides goes along with a noticeable decline of the normalized IR area of carbonate groups, that is, normalized IR areas are lower than the ones predicted for the straight line in Fig. 6. This last observation is also an indication that we are not in the presence of mechanical mixtures or composite of pure grains of ceria and gallia.

Now, to obtain a more detailed picture of the changes in CO_2 chemisorption on Ce–Ga oxides, it is necessary to identify the carbonate groups over the different materials to further examine their apparent fractional surface composition and thermal stability. The right assignment of the IR bands to surface carbonate species is supported by the pertinent analyses of the following features: (i) the wavenumber of the IR signals corresponding to carbonates adsorbed over other metal oxides, (ii) the width of the ν_3-band splitting of the $CO_3^=$ anion (that is, the $\Delta\nu_3 = \nu_{as} - \nu_s$ of the CO_3 stretching modes) due to the loss of its D_{3h} symmetry by chemisorption, [20,26] and (iii) the thermal evolution of the intensity of each signal (thermal stability).

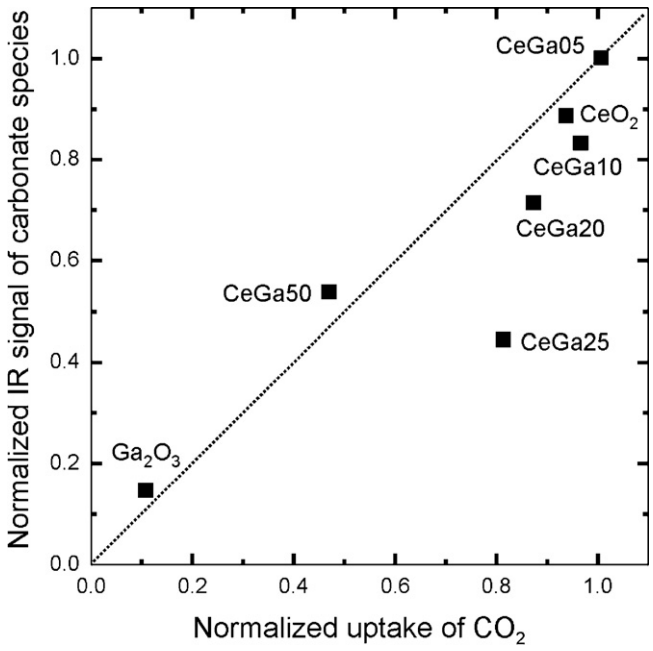

Fig. 6. Normalized integrated infrared absorbance in the 1800–1100 cm^{-1} region versus the normalized total amount of CO_2 adsorbed at 298 K measured by MS. (The IR absorption values were interpolated at 37 Torr CO_2 from the data of Fig. 5.)

Temperature-programmed desorption (TPD) experiments followed by infrared spectroscopy between 298 and 723 K ($\beta = 5\ K\ min^{-1}$) were performed under dynamic vacuum after the isothermal CO_2 adsorptions at 298 K. Representative carbonate infrared spectra, including the infrared region of the OH bond stretching, are displayed in Fig. 7 for the whole set of studied material at 298, 473 and 723 K under vacuum. Finally, Fig. 8 summarized the thermal evolution of the carbonate region (1800–1100 cm^{-1}) during the TPD.

3.3.1. Carbonate groups on gallia

A complete and careful identification of the surface carbonate infrared peaks was done by some of us over a series of different pre-reduced polymorph of gallia with varying BET surface areas [27].

Accordingly, after the analysis of the infrared spectra collected during the adsorption of CO_2 and the temperature programmed desorption on our pre-reduced and subsequently pre-oxidized γ-Ga_2O_3 sample of the present work, the following carbonate species were identified: bicarbonate [HCO_3^-: $\nu_{as}(CO_3) = 1629\ cm^{-1}$, $\nu_s(CO_3) = 1427\ cm^{-1}$ and $\delta(OH) = 1228\ cm^{-1}$], monodentate carbonate [$\nu_{as}(CO_3) = 1510\ cm^{-1}$; $\nu_s(CO_3) = 1347\ cm^{-1}$], bidentate carbonate [$\nu_{as}(CO_3) = 1591\ cm^{-1}$; $\nu_s(CO_3) = 1306\ cm^{-1}$], and polydentate carbonate [$\nu_{as}(CO_3) = 1452\ cm^{-1}$; $\nu_s(CO_3) = 1400\ cm^{-1}$].

Similar evolutions of the carbonaceous species were observed with the increase of the CO_2 pressure over both a pre-reduced [27] and our pre-oxidized gamma gallia. Moreover, after evacuation of the IR cell at 298 K (base pressure = 1×10^{-4} Torr) the intensity of most of these bands lost intensity and, finally, after 30 min of evacuation, approximately 32% of the initial total integrated signal was preserved. Thus, as in the case of only pre-reduced gallia, a moderate interaction between the CO_2 molecule and the mild O_2^- and OH^- basic centers on the surface of Ga_2O_3 is observed.

However, three main differences can be found between the previously reported pre-reduced [27] and our pre-oxidized gallia polymorph. First, after following the trends of the carbonate species on ceria (see next section) and the TPD spectra, monodentate carbonate groups (m-$CO_3^=$) is now identified on the pre-oxidized gallia surface (Fig. 7) instead of br-$CO_3^=$ on pre-reduced γ-Ga_2O_3. Second, bidentate bicarbonate groups (b-HCO_3^-), in place of monodentate bicarbonate (m-HCO_3^-), are predominant on pre-oxidized gallia during the CO_2 adsorption from 1 to 760 Torr, and the TPD experiments. Third, the signals previously attributed to carboxylate ($CO_2^{\delta-}$, $\nu_{as} = 1750\ cm^{-1}$ and $\nu_{as} = 1170\ cm^{-1}$) and bridge-carbonate (br-$CO_3^=$, $\nu_s = 1280\ cm^{-1}$ and $\nu_{as} = 1680\ cm^{-1}$) groups [27], are absent at any CO_2 partial pressure on our pre-oxidized gallia.

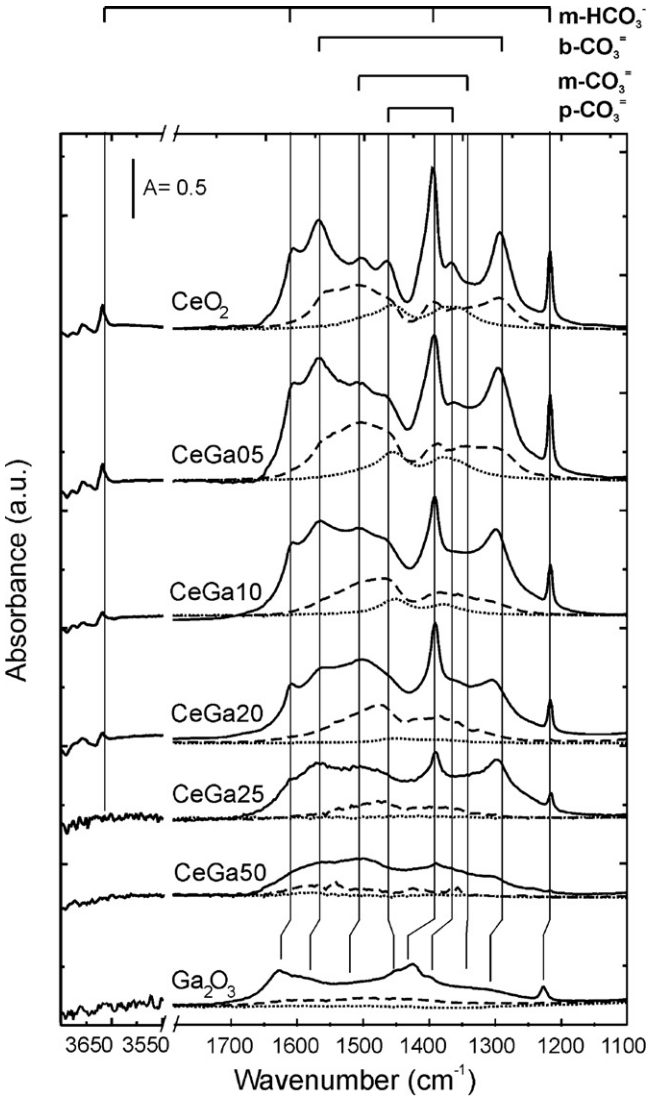

Fig. 7. Infrared spectra during the TPD experiments for the whole set of ceria–gallia and reference samples at selected temperatures: 298 K (solid line), 473 K—except for Ga_2O_3, which is 373 K—(dashed line) and 723 K (dotted line). The spectra were corrected by wafer weight and surface area of each sample.

Even though it seems difficult to find an explanation to these last three experimental observations, it is logical to assume that the particular behavior of the gallium oxide surface rests on the different pre-treatments of the sample. In regard to the formation $CO_2^{\delta-}$ groups, it has been proposed that η^2-CO_2 complex (η^2-C,O bonds) on gallia can be stabilized by (i) back-bonding between d orbitals of the Ga^{3+} ion ($3d^{10}$) and the π^* orbitals of a C=O bond of CO_2 or (ii) interaction between electron donor sites (e.g., partially reduced gallium cations, $Ga^{\delta+}$, with $\delta < 2$) which were generated by the activation of the oxide [27] and the CO_2 molecule. The present results, then, confirm the need of partially reduced gallium cations for the formation of carboxylate species. This could be probably the case also for the formation of br-$CO_3^=$, that is one of the oxygen

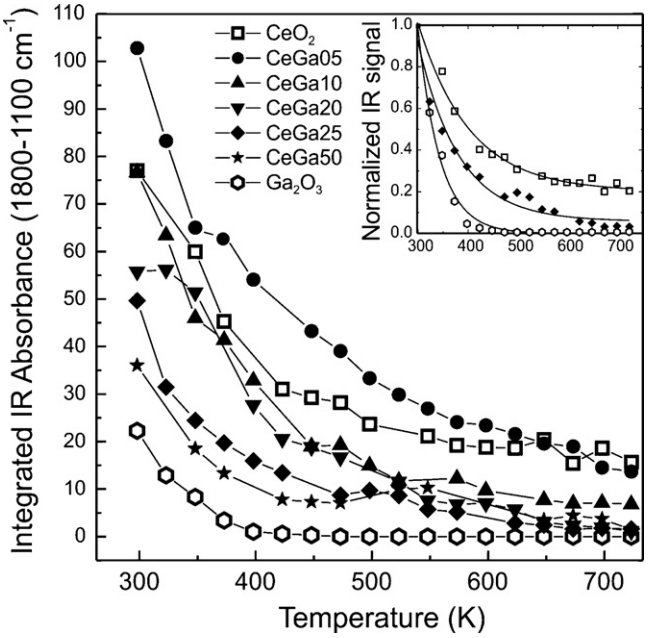

Fig. 8. Evolution of the integrated absorbance signals of the carbonate IR region (1800–1100 cm^{-1}) during the TPD experiments from 298 to 723 K for the whole set of ceria–gallia samples (10 K min^{-1}, base pressure = 1×10^{-4} Torr).

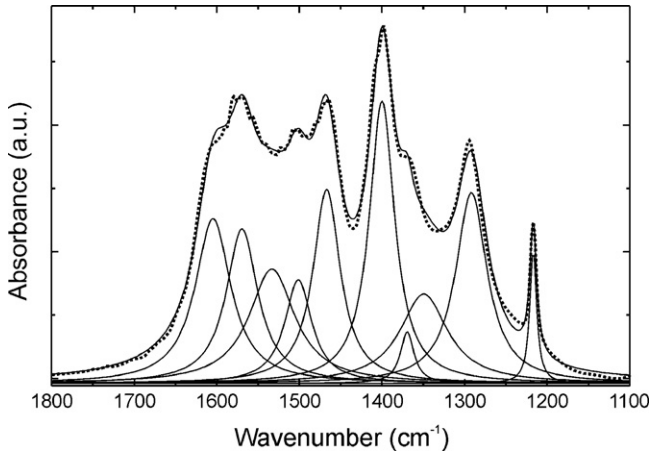

Fig. 9. Resolved infrared spectrum in the 1800–1100 cm^{-1} region corresponding to the absorption bands of the carbonate and bicarbonate species on the surface of the CeO_2 sample: experimental data (dotted line), and fitting result (solid lines).

atom of carbon dioxide would need an electron donor site ($Ga^{\delta+}$) beside a surface O_2^- basic site. Thus, the activation of gallia with molecular oxygen, which led to fully oxidized Ga^{3+} cations, will be unable to produce either carboxylate or bridge carbonate species. However, m-$CO_3^=$ groups would not require more than one surface oxygen site, and it would not be a concern in a pre-oxidized gallium oxide sample.

During the temperature ramp, bands due to bicarbonate rapidly lost intensity and vanished at 373 K. Only weak signals ascribed to bidentate and polydentate carbonate groups remained at higher temperatures, but those bands completely disappeared at 473 K (Fig. 7). Then, a very weak thermal stability of the surface carbonate species on the gallia surface is observed.

Hence, we can conclude that there is an excellent agreement among the wavenumber assignations (Table 2) and the thermal stability of the different carbonate groups residing on our pretreated gamma gallia and those reported in Ref. [27].

As regards the apparent fractional composition of the various carbonate species, a detailed analysis is presented for all the samples in the next section.

3.3.2. *Carbonate groups on ceria based oxides*

Upon CO_2 adsorption at 298 K, CeO_2 is able to form large amounts of carbonate species (Fig. 4). About the 50% of the total integrated absorbance of all these bands remained in the spectra after evacuation at room temperature, indicating, as expected, a stronger basicity of CeO_2 surface sites, as compared to that found in pure gallia. After evacuation, the spectrum of pure CeO_2 shows better resolve peaks due to the partial desorption of some carbonate species (Fig. 7). The resulting spectrum is in agreement with literature data [16]. As an example, Fig. 9 shows a typical resolved spectrum in carbonate IR region of the CeO_2 sample.

For the identification of the carbonate species on ceria, the evaluation of thermal stability of the IR signals in TPD spectra is useful (Fig. 7). During the heating ramp, three sharp peaks at 1608, 1396 and 1217 cm^{-1}, simultaneously decrease until vanishing at 423 K. Additionally, a peak at 3617 cm^{-1} in the ν(OH) region, also lost intensity with a similar evolution. In regards to the well-defined δ(OH) band at ca. 1220 cm^{-1} and to the $\nu_{as}(CO_3)$ band at ca. 1600 cm^{-1} (Figs. 4 and 7), it appears that the bicarbonate species on pure ceria are similar to those on pure gallia (see Table 2). The position and thermal stability of these bands allow to assign them to bicarbonate species, HCO_3^-: $\nu_{as}(CO_3)$ = 1608 cm^{-1}, $\nu_s(CO_3)$ = 1396 cm^{-1}, δ(OH) = 1217 cm^{-1} and ν(OH) = 3617 cm^{-1}. The ν_3-band splitting of the species, 212 cm^{-1}, is in agreement with that of adsorbed bicarbonates (ca. 200 cm^{-1}) on different metal oxides [26–31].

Actually, two signals corresponding to the $\nu_s(CO_3)$ mode of HCO_3^- species were registered [20,27]. These bands can be easily discerned in the spectra at 1 and 760 Torr CO_2 (Fig. 4). Together with the band at 1396 cm^{-1}, another one at 1419 cm^{-1} showed up, and their relative intensities changed after increasing the CO_2 pressure. After evacuation, the signal at 1419 cm^{-1} almost vanished, which shows a lower stability for that species, while the peak at 1396 cm^{-1} remained up to 473 K. Accordingly, Binet et al. reported two types of bicarbonate (or hydroxy carbonate) species on CeO_2, named I and II [16], which were distinguished one each other by the different position of the $\nu_s(CO_3)$ mode at 1413 and 1391 cm^{-1}, respectively. Species I vanished upon evacuation at room temperature, while a temperature equal to 373 K was needed to eliminate species II. These thermal behaviours are similar to the ones observed for the bands at 1419 and 1396 cm^{-1} on our cerium dioxide (and also on the Ce–Ga oxides). Thus, it is reasonable to assign the previous last bands to bidentate (b-HCO_3^-) and monodentate (m-HCO_3^-) carbonate groups, respectively.

Besides the bicarbonate species, other carbonate groups can be detected on the surface of ceria. A couple of strong bands at 1570 and 1294 cm^{-1} progressively lost intensity to fade out at 573 K. These bands are ascribed to the $\nu_{as}(CO_3)$ and $\nu_s(CO_3)$ modes of bidentate carbonate species (b-$CO_3^=$), because their band splitting ($\Delta\nu_3$ = 276 cm^{-1}) is in close agreement to the 300 cm^{-1} splitting found for such species over other metal oxides [20,27,32–34].

A more complex set of bands, highly overlapped, is present in the 1550–1450 cm^{-1} region. The most stable signals at ca. 1462 and 1366 cm^{-1} ($\Delta\nu_3$ = 96 cm^{-1}) remain in the spectrum at 723 K. They were highly overlapped at low temperature, but became clearly visible when all the other carbonate signals faded out at about 673 K (see Figs. 4 and 7). These bands could account for the presence of either monodentate (m-$CO_3^=$) or polydentate carbonate (p-$CO_3^=$) species, which have similar ν_3-band positions and close $\Delta\nu_3$ to about 100 cm^{-1} [20,26,27,32–34]. However, these carbonate groups present different thermal stability, the surface m-$CO_3^=$ should be much less stable than the p-$CO_3^=$ [20,26]. Therefore, due

Table 2
Wavenumber of the infrared bands of (bi)carbonate species on the surface of CeO_2, Ga_2O_3 and Ce–Ga mixed oxides.

	HCO_3^-					m-$CO_3^=$		b-$CO_3^=$		p-$CO_3^=$	
	$\nu_{as}(CO_3)$	$\nu_s(CO_3)$		δ(OH)	ν(OH)	$\nu_{as}(CO_3)$	$\nu_s(CO_3)$	$\nu_{as}(CO_3)$	$\nu_s(CO_3)$	$\nu_{as}(CO_3)$	$\nu_s(CO_3)$
		Monodentate	Bidentate								
CeO_2	1608	1396	1419	1217	3617	1504	1344	1570	1294	1462	1366
CeGa05	1609	1396	1418	1217	3618	1512	1341	1570	1295	1465	1362
CeGa10	1609	1396	1419	1217	3617	1510	1344	1568	1298	1466	1366
CeGa20	1611	1393	1430	1217	3617	1508	1344	1566	1303	1463	1366
CeGa25	1608	1395	1415	1217	3617	1507	1342	1565	1302	1466	1365
CeGa50	1609	1393	1422	1215	3617	1502	1344	1572	1303	1444	1366
Ga_2O_3	1629	1427	–	1228	–	1510	1347	1591	1306	1452	1400

to the strong thermal resistance, the signals at 1462 and 1366 cm^{-1} are attributed to the $\nu_{as}(CO_3)$ and $\nu_s(CO_3)$ modes, respectively, of multiple bonded CO_2 over the cerium oxide surface, that is, polydentate carbonate species.

There is, finally, an additional couple of bands at 1504 cm^{-1} and 1344 cm^{-1}, which showed a lower thermal stability than the previous ones, and lost most of their intensity after evacuation at 673 K. These last two peaks are assigned to monodentate carbonate on ceria [$\nu_{as}(CO_3)$ = 1504 cm^{-1}; $\nu_s(CO_3)$ = 1344 cm^{-1}] [20,26].

Concerning the Ce–Ga mixed oxides (up to 25% mol/mol of Ga), the results presented before have broadly shown a decreasing tendency of the total amounts of adsorbed CO_2 as the gallium content increases into the cerium based samples (Figs. 3–6). Spectra recorded during the isothermal adsorption of CO_2 over the Ce–Ga mixed oxide series, qualitatively shows that the spectral features progressively change as the gallium loading increases (Fig. 4). The same criteria described above were employed to resolve the overlapped bands and to assign each carbonate species in the mixed oxides. Table 2 summarizes the bands of the different carbonate species for each Ce–Ga mixed oxides. It is observed that the characteristic wavenumbers of each surface (bi)carbonate group on Ce–Ga mixed oxides are almost identical to those on pure ceria.

To analyze the differences in the basic surface sites, Fig. 10 shows the apparent fraction distribution of the carbonate species for each oxide at 100 Torr CO_2 and under vacuum at 298 and 473 K.

Whether CO_2 is present in the gas phase or not, in regards to the monodentate and polydentate carbonate groups, there is a moderate increase in their apparent surface fraction as the amount of gallium incorporated into the lattice ceria increased. An opposite trend is observed for the relative amounts of b-$CO_3^=$ and HCO_3^- species. Again, the CeGa50 does not follows those trends since, as expected, it is an heterogeneous sample, probably a composite material, exposing partially pure CeO_2 and Ga_2O_3, as well solid solution of Ce–Ga oxides.

Fig. 10 also reveals that the apparent fraction of HCO_3^- and m-$CO_3^=$ were the most influenced after the evacuation, but in opposite directions. For example, on the surface of the CeGa25 sample the fraction of bicarbonate groups decreases approximately 40%, but the relative amount of monodentate carbonate increases approximately 45%. The fractions of the other carbonates groups rest almost unchanged. The increase of the temperature up to 473 K showed that the Ce–Ga mixed oxides have a surface enriched with m-$CO_3^=$ and p-$CO_3^=$, and in a higher level for the richer gallium samples, that is, CeGa20 and CeGa25. In other words, the incorporation of gallium(III) cations into ceria lattice weaken the carbonate species on the surface of the new materials, remaining mostly the strongly bonded surface carbonate groups at 473 K.

3.3.3. Thermal stability of carbonate groups

Fig. 8 shows the thermal evolution of the carbonate species over the whole set of samples during the TPD experiments. On one side, carbonate group concentration noticeably decreases with the

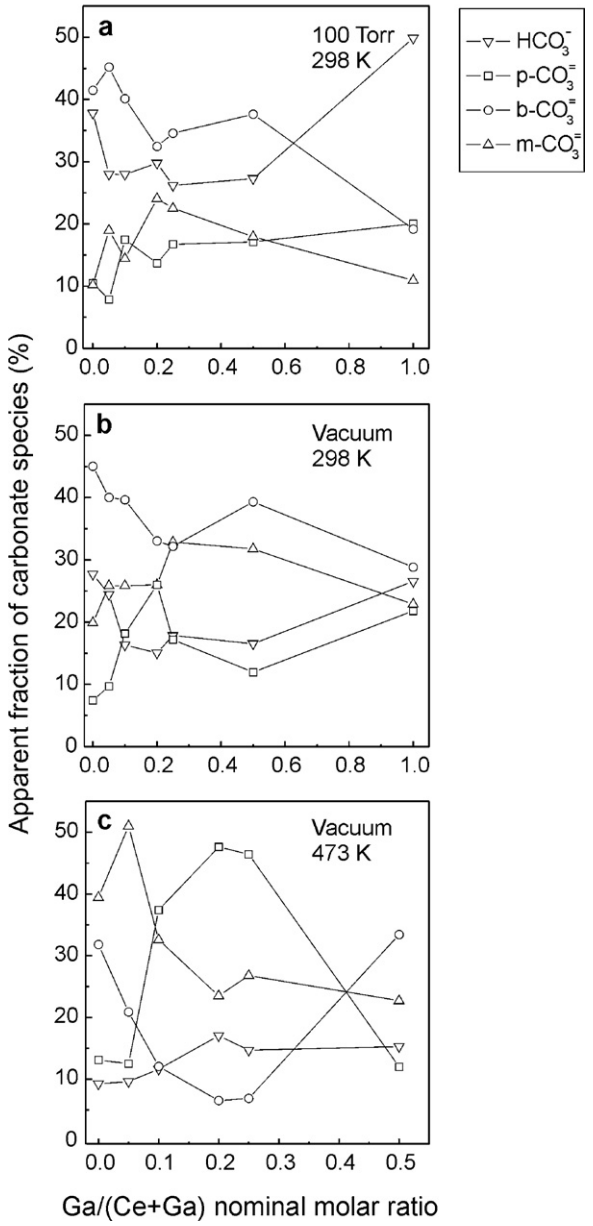

Fig. 10. Relative amounts of the different carbonate surface species as a function of the gallium content in the whole set of ceria–gallia samples: 100 Torr CO_2 (a) and under vacuum (20 min) at 298 K (b), and during the TPD experiment at 473 K (c).

incorporation of gallium into the ceria matrix. But, on the other side, it can be observed that not only the concentration but also the decomposition rate of the surface (bi)carbonate species are different. The thermal evolution of the normalized integrated IR absorbance for the carbonate groups on CeO_2, CeGa25 and Ga_2O_3, which is showed in the inset of Fig. 8, supports the conclusion that the carbonate species, in general, are faster removed on the Ce–Ga mixed oxides than on pure ceria. A detailed spectral evolution with the temperature can be found in Fig. 1 of the Supplementary Data for the same selected three samples (that is, ceria, CeGa25 and gallia). For pure cerium oxide almost all adsorbed bicarbonates have been eliminated at 473 K, while bidentate carbonates are removed at 573 K, and only polydentate carbonate species remained at the highest temperature. On the contrary, the thermal stability of carbonate species on pure Ga_2O_3 is significantly lower than in the ceria: no carbonates species can be detected over 400 K.

As regards to the thermal evolution of carbonaceous species on the surface of the mixed oxides, a decrease of the overall stability can be appreciated as compare to ceria. It seems that the stability of the bicarbonate species is the only one not significantly modified by the addition of gallium to cerium oxide, because these surface groups disappeared at ca. 473 K (see Fig. 1a and b in the supplementary data). However, bidentate carbonate groups are more labile with the increase of gallium loading, remaining on the surface up to 548, 523, 498 and 473 K in CeGa05, CeGa10, CeGa20 and CeGa25. A similar behavior was also observed for monodentate and polydentate carbonate groups, their thermal stability is also influenced negatively as the gallium loading increases. For CeGa05 and CeGa10, p-$CO_3^=$ are relatively stable even at 723 K. However, for samples with more than 10% mol/mol of Ga, those groups vanish from 698 K. Therefore, a lower coverage of less stable polydentate carbonate groups is produced in the gallium doped-ceria system.

4. Conclusions

A set of cerium–gallium mixed oxides was prepared by co-precipitation with ammonium hydroxide in aqueous phase, with composition ranging from 5 to 50% mol/mol of Ga. All the Ce–Ga oxides, after calcination at 773 K, were mesoporous with BET surface areas from 75 to 104 m^2/g. Based on the molecular weight of the oxides, the values of BET surface areas were very close, up to 25% mol/mol of Ga, while it was a 30% lower for the CeGa50 material. Only a fluorite-type crystal structure of CeO_2 was detected for all ceria based samples. After the addition of gallium(III), a consistent shift of the CeO_2 (1 1 1) diffraction peak near 28°, that is, a contraction of the lattice parameter, indicates that the solubility of gallium (III) in ceria is close to 25% mol/mol of Ga. The structural and morphological–textural analysis also suggested that the CeGa50 sample is a heterogeneous material.

Total CO_2 uptake was used to measure the global basicity of the Ce–Ga oxide system. A moderated decrease in the amount of carbon dioxide adsorbed (partial pressure = 37 Torr CO_2) was observed as the Ga molar content increased in the Ce–Ga mixed oxides.

Diverse surface carbonate species were identified by infrared spectroscopy. These species formed in the surface of Ce–Ga mixed oxides vibrate at wavenumbers similar to the ones on pure ceria surface rather than those on pure gallia. However, a change in the relative distribution of the carbonate groups was observed as the gallium content increased into the ceria matrix. Mainly, a moderate enrichment of the apparent concentration of m- and p-$CO_3^=$ groups and a significant decrease in the relative amount of b-$CO_3^=$ and HCO_3^- species were observed along the gallium content increased in the cerium-based mixed oxide.

For the set of cerium-based materials the order of thermal stability found for the various carbonaceous species is as follows: HCO_3^- < b-$CO_3^=$ ~ m-$CO_3^=$ < p-$CO_3^=$. At its turn, all those species are less stable on gallium-doped oxides than on pure cerium dioxide. Thus, the formation of more labile carbonate species indicates that the Ce–Ga–O system could yield an appropriated support for catalysts to be applied for the low-temperature water gas shift reaction and the CO preferential oxidation in a hydrogen reach stream for hydrogen purification.

Acknowledgements

This work was supported by the National Council for Scientific and Technical Research (CONICET), the National Agency for the Promotion of Science and Technology (ANPCyT, Grant PICT 2005 14-33101), and Universidad Nacional del Litoral (CAID J379) of Argentina, the Spanish International Cooperation Agency (PCI-AECID, Project A-026518-09), the EULANEST 042 project. Likewise, we acknowledge the financial support from MCINN of Spain/FEDER-EU (Project No: MAT2008/00889-NAN). G.F. thanks CONICET for the research fellowship received to do her work.

Appendix A. Supplementary data

Supplementary data associated with this article can be found, in the online version, at doi:10.1016/j.cattod.2011.04.054.

References

[1] A. Trovarelli (Ed.), Catalysis by Ceria and Related Materials, Imperial College Press, London, 2002.
[2] G.C. Bond, C. Louis, D.T. Thompson (Eds.), Catalysis by Gold: Catalytic Science Series, vol. 6, World Scientific Publishing Co., London, 2006.
[3] Q. Fu, W. Deng, H. Saltsburg, M. Flytzani-Stephanopoulos, Appl. Catal. B 56 (2005) 57–68.
[4] R. Burch, Phys. Chem. Chem. Phys. 8 (2006) 5483–5500.
[5] W. Deng, M. Flytzani-Stephanopoulos, Angew. Chem. Int. Ed. 118 (2006) 2343–2347.
[6] Y. Denkwitz, A. Karpenko, V. Plzak, R. Leppelt, B. Schumacher, R.J. Behm, J. Catal. 246 (2007) 74–90.
[7] A. Karpenko, R. Leppelt, J. Cai, V. Plzak, A. Chuvilin, U. Kaiser, R.J. Behm, J. Catal. 250 (2007) 139–150.
[8] A. Goguet, R. Burch, Y. Chen, C. Hardacre, P. Hu, R.W. Joyner, F.C. Meunier, B.S. Mun, D. Thompsett, D. Tibiletti, J. Phys. Chem. C 111 (2007) 16927–16933.
[9] A. Karpenko, Y. Denkwitz, V. Plzak, J. Cai, R. Leppelt, B. Schumacher, R.J. Behm, Catal. Lett. 116 (2007) 105–115.
[10] A. Abd El-Moemen, A. Karpenko, Y. Denkwitz, R.J. Behm, J. Power Sources 190 (2009) 64–75.
[11] S.E. Collins, G. Finos, E. del Rio, R. Alcantara, S. Bernal, A.L. Bonivardi, Appl. Catal. 388 (2010) 202–210.
[12] S. Bernal, G. Blanco, J.M. Gatica, J.A. Pérez-Omil, J.M. Pintado, H. Vidal, G.A. Adachi, N. Imanaka, Z. Kang (Eds.), Binary Rare Earth Oxides, Kluwer Academic/Plenum Press, 2004, pp. 9–55 (Chapter 2).
[13] T. Yuzhakova, V. Rakic, C. Guimon, A. Auroux, Chem. Mater. 19 (2007) 2970–2981.
[14] B. Bonnetot, V. Rakic, T. Yuzhakova, C. Guimon, A. Auroux, Chem. Mater. 29 (2008) 1585–1596.
[15] J.C. Lavalley, Catal. Today 27 (1996) 377–401.
[16] C. Binet, M. Daturi, J.C. Lavalley, Catal. Today 50 (1999) 207–225.
[17] C. Binet, A. Badri, J.C. Lavalley, J. Phys. Chem. 98 (1994) 6392–6398.
[18] C. Li, Y. Sakata, T. Arai, K. Domen, K.-i. Maruya, T. Onishi, J. Chem. Soc., Faraday Trans. I 85 (4) (1989) 929–943.
[19] C. Li, Y. Sakata, T. Arai, K. Domen, K.-i. Maruya, T. Onishi, J. Chem. Soc., Faraday Trans. I 85 (6) (1989) 1451–1461.
[20] G. Busca, V. Lorenzelli, Mater. Chem. 7 (1982) 89–126.
[21] S.E. Collins, M.A. Baltanás, A.L. Bonivardi, Langmuir 21 (2005) 962–970.
[22] C. Otero Areán, A. López Bellan, M. Peñarroya Mentruit, M. Rodríguez Delgado, G. Turnes Palomino, Micropor. Mesopor. Mater. 40 (2000) 35–42.
[23] J. Vecchietti, S. Collins, J. Delgado, M. Małecka, E. del Rio, X. Chen, S. Bernal, A. Bonivardi, Top. Catal 54 (2011) 201–209.
[24] D. Briggs, M.P. Seah, Practical Surface Analysis, 2nd ed., vol. 1, John Wiley & Sons Press, 2002.
[25] M. Calatayud, private communication.
[26] K. Nakamoto, Infrared and Raman Spectra of Inorganic and Coordination Compounds, Wiley, New York, 1996.
[27] S.E. Collins, M.A. Baltanás, A.L. Bonivardi, J. Phys. Chem. B 110 (2006) 5498–5507.
[28] B. Bachiller-Baeza, I. Rodriguez-Ramos, A. Guerrero-Ruiz, Langmuir 14 (1998) 3556–3564.

[29] K. Pokrovski, K. Jung, A.T. Bell, Langmuir 17 (2001) 4297–4303.
[30] A.A. Davydov, M.L. Shepotíko, A.A. Budneva, Kinet. Catal. 35 (1994) 272–278.
[31] R. Philipp, K.J. Fujimoto, Phys. Chem. 96 (1992) 9035–9038.
[32] C. Morterra, G. Magnacca, Catal. Today 27 (1996) 497–532.
[33] F. Ouyang, K. Nakayama, K. Tabarda, E.J. Suzuki, J. Phys. Chem. B 104 (2000) 2012–2018.
[34] A.A. Davydov, V.G. Mikhaltchenko, V.D. Sokolvskii, G.K. Boreskov, J. Catal. 55 (1978) 299–313.